https://erjm.journals.ekb.eg
ISSN: 1110-1180

DOI: ---------

ERJ
Engineering Research Journal
Faculty of Engineering
Menoufia University

Investigating a Modified Vertical Axis Wind Turbine

Sarah Eltahwihy[1], Ali M. Abdelsalam[2], Ismail M. Sakr[2]* , Kamal A. Ibrahim[2]

[1]*MSc. Candidate, Dept. of Mech. Power Eng., Menoufia University, Shebin El-Kom, Egypt.*
[2]*Mechanical Power Eng. Depart., Faculty of Eng., Menoufia University, Shebin El-Kom, Egypt.*
[*]*(Corresponding author: ismailsakr@yahoo.com)*

ABSTRACT
This investigation aims to analyze experimentally and numerically the performance of the Savonius wind turbine with a modified blade shape/profile. The wind turbine rotor introduced consists of two hook-shaped buckets connected by a Batch/arm with different bucket orientations. Blades of the cross-section with different thicknesses are considered. The simulations are carried out using the three-dimensional incompressible unsteady Reynolds-Average Navier Stokes (RANS) equations along with the RNG *k-ε* turbulence model. The results indicate that the RNG *k-ε* turbulence model achieves a good prediction of the rotor performance, in comparison with the literature and the current measurements. Six rotor models are investigated to explore the effect of rotor shape along with blade thickness on the wind turbine performance. It is revealed that the rotor model with a blade thickness of 2 mm and bucket orientation with a parallel arm-bucket, Model 4, has the best performance among the tested rotors. The static torque shows positive values for all rotor angles with a maximum static torque coefficient of 0.45, which reveals the high starting ability of the present rotor.

Keywords: *Savonius Rotor; Blade profile; Wind turbine performance; Arm length.*

1. Introduction

The Savonius rotor is a drag-based vertical axis wind turbine whose operating theory depends on the difference in drag force between the convex and concave surfaces of the rotor blades. Savonius wind turbines have many advantages, including simple construction, low cut-in wind speed, no need to orient towards wind direction, good self-starting ability, low noise, and low maintenance. However, the performance of Savonius rotors is lower than other conventional wind rotors. Hence, numerous researchers carried out experimental and numerical studies to reach a design of a higher power coefficient C_p, which is the ratio of the rotor power to the power available in the wind. The design parameters of the Savonius rotor are extensively tested in the literature to optimize its values. It is found that the two blades rotor is more efficient than three and four blades [1-2]. Blades with an overlap 0.15 of chord length achieve higher performance [2]. The rotor with end plates gives higher efficiency than those without endplates [1], and the use of both upper and lower endplates was found to increase the power coefficient by 36 % [1].

Twisting the rotor blades has a significant effect on the turbine performance, and has been examined by numerous authors. El-Askary et al. [3] examined the power coefficient C_p and the torque coefficient C_T at blade twist angles from 0 to 180°. The torque coefficient is a non-dimensional measure of the torque produced by the wind turbine rotor. They found that the optimum twist angle of the modified rotor is 45°, where C_{Pmax} and C_{Tmax} are 0.22 and 0.41 respectively. Damak et al. [4] studied the effect of the Savonius helical rotor with a twist of 180° on rotor performance and reached that, helical blades provided better performance than conventional ones. Al-Faruk and Sharifian [5] explored a new hybrid design of swirling Savonius turbine rotor and reported an increase of 24.12 % in the power coefficient compared to the optimum conventional Savonius turbine. It is indicated that the maximum power coefficient occurred at tip speed ratios from 0.4 to 0.8 (ratio of the rotor speed at the blade tip to the inflow wind speed) while C_{Pmax} and C_{Tmax} occurred at a twist angle of 45°. Lee et al. [6] indicated that the maximum power coefficient is

achieved at 45° twist angle. The same optimum twist angle of 45° was also reported for the modified blade profile [3].

The blade shape also plays a basic role in extracting energy from the wind efficiently. Different shapes of blade profiles were proposed in the literature. The elliptical Savonius rotor performed better than the Bach-type and the classical Savonius rotor in the range of tip speed ratio between 0.2 and o.4 [7]. Roy and Saha et al. [8] studied different types of blades including semi-circular, semi-elliptic, Benesh, and Bach types. It was found that the torque and power coefficients C_T and C_P are higher for their newly developed blade profiles. The helical Bach rotor had the highest power coefficient and static torque coefficient as compared to the helical rotor. The power coefficient for the helical Bach rotor reported 0.2 while it was 0.18 for the helical one [9]. Alom and Saha [10] studied different blade shapes of Savonius wind turbine; twisted, elliptic, Roy, Batch, semicircular, and new elliptical, and found that the Roy profile improved the starting torque by 31.6 % compared to the conventional semicircular profile. Pranta et al. [11] proposed a Savonius blade of the straight section along with a tangent arc. Their 2-D numerical simulations showed an 18% increase in the power coefficient as compared to the conventional rotor. Different optimization techniques were also employed on many rotor designs [12, 13]. However, there were no overarching conclusions about the effect of the various geometrical parameters on the rotor performance. A recent review on the effect of geometrical parameters on the maximum power and torque coefficient of the Savonius rotor is conducted by Cuevas-Carvajal et al. [14].

The application of effective design of small vertical axis wind turbine to allow producing energy in small spaces even at low wind speed is currently under development. In the present work, a modified blade shape of the Savonius rotor is proposed, considering arm-buckets of different orientations and two thicknesses. The performance of the wind turbine rotor is investigated numerically and experimentally. Experiments are conducted for validation purposes.

2. Present Rotor Configurations

The rotor geometry presented in this paper consists of two buckets with a hook-shape profile [15] connected by the Batch arm of a fixed length of 4.3 cm. Six rotor geometries, shown in Figure 1, are investigated with changing bucket length, thickness, and orientation. The aspect ratio (AR), which is the rotor height to the rotor diameter, is fixed as AR = 1 for all rotors. The rotor model M2 is the same as the rotor model M1 however with a reduction in the bucket length at its outer edge, as shown in Figure 1-a and Figure 1-b. The rotor model M3 has blade thickness of 2 mm with bucket profile like model M1. For rotor model M4, the two buckets are hooked towards the outer edge of the rotor. Furthermore, the first four models M1, M2, M3, and M4, the rotor arm is parallel to the blade chord, while it is perpendicular to the blade chord for models M5 and M6.

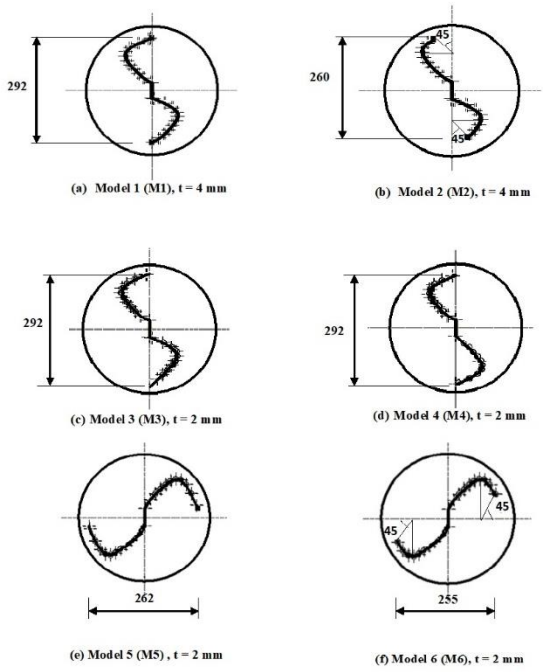

Figure 1- Savonius rotor models under investigation

3. Numerical Technique

The airflow around the wind turbine rotor is considered unsteady three-dimensional incompressible flow. Hence, the 3-D unsteady Reynolds Average Navier Stokes (URANS) equations are used [16-18]. Ansys Fluent 17.0 is employed in the present study and the SIMPLE algorithm is utilized for pressure velocity coupling. The second-order upwind scheme is selected for improving simulation accuracy. The airflow is characterized by turbulent fluctuations and hence turbulence modeling is required. The RNG *k-ε* turbulence model is proved to predict well the Savonius rotor performance [16-18]. Consequently, it is used in the present simulations. The RNG *k-ε* model includes additional formulations for the turbulent viscosity μ_t and for the dissipation rate ε which have low effects on the Reynolds number. The transport equations for turbulent kinetic energy *k* and its dissipation rate ε are given as;

$$\frac{\partial}{\partial t}(\rho k) + \nabla.\left(\rho k u_i\right) = \nabla.\left[\left(\mu + \frac{\mu_t}{\sigma_k}\right)\nabla k\right] + G_k - \varrho\epsilon + S_k \quad (1)$$

Specific dissipation rate ω-equation

$$\frac{\partial}{\partial t}(\rho\varepsilon) + \frac{\partial}{\partial x_i}\left(\rho\varepsilon u_i\right) = \frac{\partial}{\partial x_j}\left[\left(\mu + \frac{\mu_t}{\sigma_\varepsilon}\right)\frac{\partial\varepsilon}{\partial x_j}\right] + C_{1\varepsilon}\frac{\varepsilon}{k}\left(G_k + C_{3\varepsilon}G_b\right) - C_{2\varepsilon}\rho\frac{\varepsilon^2}{k} + S_\varepsilon \quad (2)$$

where ρ is the air density, u_i is the velocity, G_k represents the generation of turbulence kinetic energy due to the mean velocity gradients, $C_{1\varepsilon}$, $C_{2\varepsilon,}$and $C_{3\varepsilon}$ are model constants. σ_ε is the inverse effective Prandtl numbers for ε. S_k, and S_ε are user-defined source terms. The computational domain is divided into two regions, the first one is the rotating domain around the rotor which involves Savonius rotor and the second is the stationary domain, see Figure 2. The computational domain's three-dimensional CAD model was completed using Inventor program, and the computational grids were created using the ANSYS ICEM program with unstructured mesh as shown in Figure 3. The computational domain is spatially discretized by tetra cells to solve the Unsteady Reynolds-Averaged Navier-Stokes (URANS) equations using finite volume method. Over the rotor blades the non-dimensional near-wall grid distance (y+) is kept less than 5.

3.1 The computational domain and boundary conditions

The dimensions of the computational domain are shown in Figure 2, relative to the turbine diameter (D). The computational domain consists of a cylindrical rotating mesh bounded the turbine rotor. This cylindrical zone (interface) has a diameter 1.25 D and a height 1.1D. The lateral sides of the computational domain have a 5D distance and also the top and bottom sides have the same distance. The domain dimensions provide a 4% blockage ratio which is below the range of 6–7.5% that has a negligible effect on the flow [18]. The inlet boundary is set 2D upstream of the rotor with uniform wind speed, and 5% turbulence intensity is used (chosen from experimental data). The 2D distance was recommended by earlier researchers who have showed the effect of the upstream distance on the solution accuracy [19, 20]. The outlet boundary is set 10D downstream of the rotor with zero value of the static pressure relative to the atmospheric pressure. The time step size is taken as 0.001 s for all the tip speed ratios with maximum value of the rotation angle **θ**=3.6°. The simulations are continued till achieving consistent torque from the rotor with repeated values during the further rotor cycle.

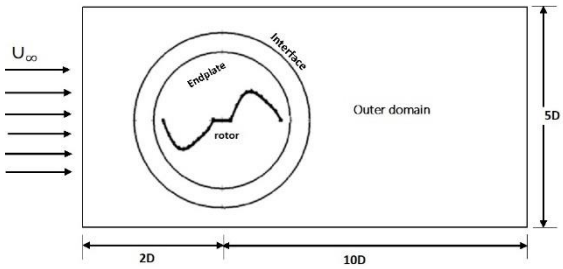

Figure 2- Schematic representation of cross section through the computational domain (not to scale)

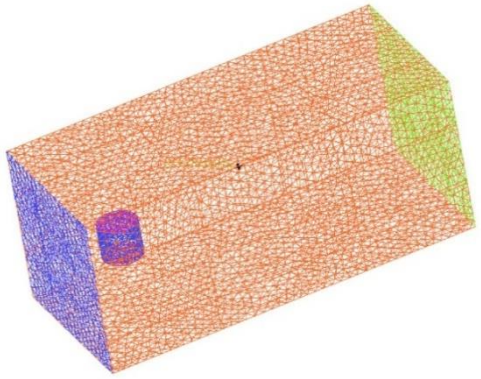

(i) 3D grid generation for the computational domain

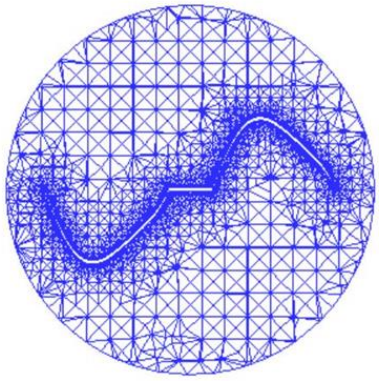

(ii) Surface mesh for cross section through

Model 1 rotor (M1).

Figure 3- The computation grid

3.2 Grid independence study and model validation

Grid independence analysis was carried out using an unstructured mesh of appropriate grid sizes with four different grid resolutions (0.5, 1.2, 2.4, and 4.8 million cells). Figure 4 shows the variation of the power coefficient with respect to the number of grid cells. It is found that 2.4 million cells are sufficient compared to a higher number of grid cells to hold minor variations in the numerical computations. Hence, the grid with 2.4 million cells is used for further simulations.

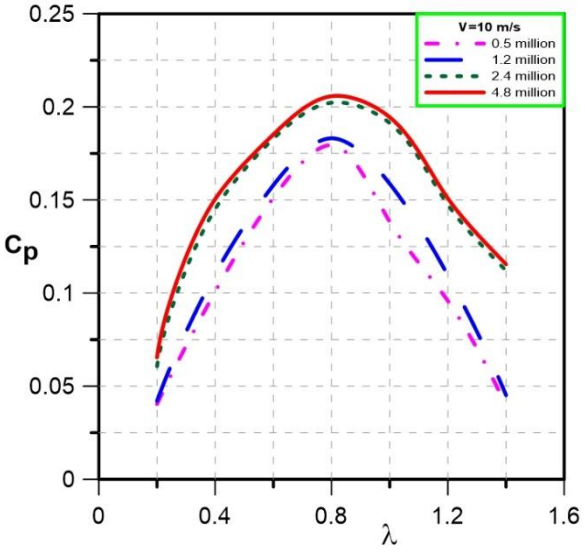

Figure 4- Grid independence study based on power coefficient variation

The present numerical methodology is validated by the experimental data presented by El-Askary et al. [3]. The rotor diameter is 400 mm and the aspect ratio is AR = 1. The simulation is performed at two inflow wind speeds.

The peak performance C_{pmax} is predicted well at an inflow wind speed of 6 m/s, as shown in Figure 5, while there is an overestimation of C_{pmax} at an inflow wind speed of 10 m/s as shown in Figure 6. Further, tip speed ratio λ = 0.8 corresponding to C_{pmax} is well achieved numerically for both wind speeds. A comparison of present numerical results and experimental data indicates a Correlation Coefficient R^2 [3] equals 0.94 at a wind speed of 6 m/s while R^2 equals 0.79 at a wind speed of 10 m/s.

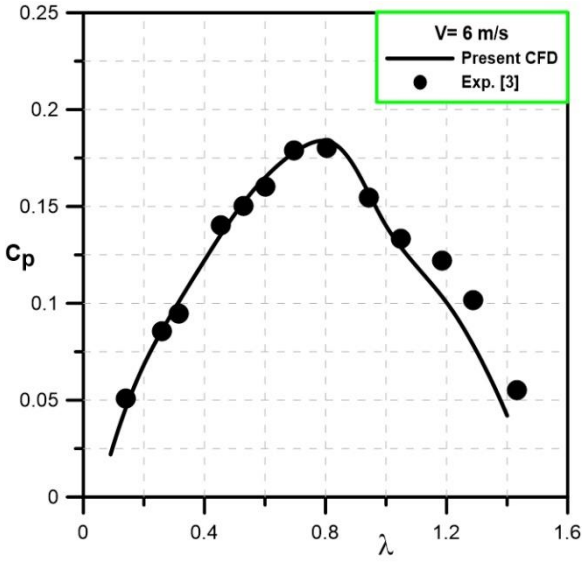

Figure 5- Comparison of Power Coefficient obtained numerically with experimental measurements of El-Askary et al. [3], V = 6 m/s

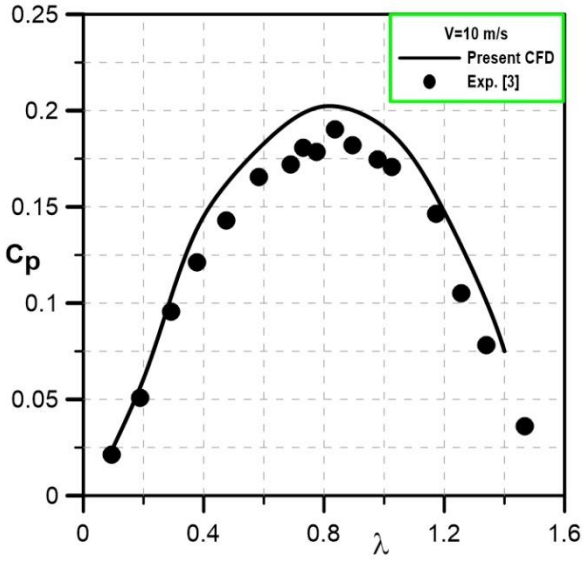

Figure 6- Comparison of Power Coefficient obtained numerically with experimental measurements of El-Askary et al. [3], V = 10 m/s

4. Experimental Test Rig

To study the wind turbine performance, a free jet test rig in the advanced fluid mechanics laboratory, Faculty of Engineering, Menoufia University is used. Figure 7 presents a photograph of the test rig used in the present work. The free jet wind tunnel uses a centrifugal fan (1) of different speeds controlled by an inverter. The maximum wind speed obtained at the tunnel exit is 12 m/s. The fan is driven by an AC motor (2) of 15 HP rated power. The circular duct (3) connected to the fan has 2-5 m in length and 1.2 m in diameter. This duct is fabricated from galvanized iron sheets of thickness of 1.5 mm. In front of the duct, the Savonius rotor (4) is placed in a structure housing fabricated from mild steel plates. The Savonius rotor projected area facing the wind is (292 mm*292 mm). The rotor is connected to the steel housing through its upper and lower endplates by a steel shaft (5) of 30 mm diameter. The blades of the rotor are made from fiberglass material by casting process while endplates are made from wood. Four ball bearings (SKF) (6) are mounted in the steel housing in order to make rotating smoothly of the Savonius rotor. The bearing is fixed with the structure housing, weighing pan (7), torque meter (8), and nylon string (9) of 1 mm diameter. The mechanical torque in (N. m) and the rotational speed in (rpm) are measured together by a digital torque meter [WinEasyTORK Manual Version 1.0 Model: MO.RT2MTOR. 541. R4]. It is a compact digital torque meter with a range of 0:25 N.m and an accuracy of 0.001 N.m. The frictional losses in the bearing have been neglected in the calculation of the power coefficient. The wind speed facing the rotor is measured horizontally and vertically through a scanning grid of 144 equal cells covering the rotor using a digital standard pitot tube (Extech HD350 Pitot Tube Anemometer + Differential Manometer) with a resolution of 0.01 m/s and accuracy of ± 0.03 m/s. This technique was also used in [21] to employ accurate wind power calculations. The wind speed is measured three times for the same condition (cell) and the average value is taken as the actual wind speed. The Savonius rotor fabricated and tested in the present work is Model M4 presented as a photograph in Figure 8.

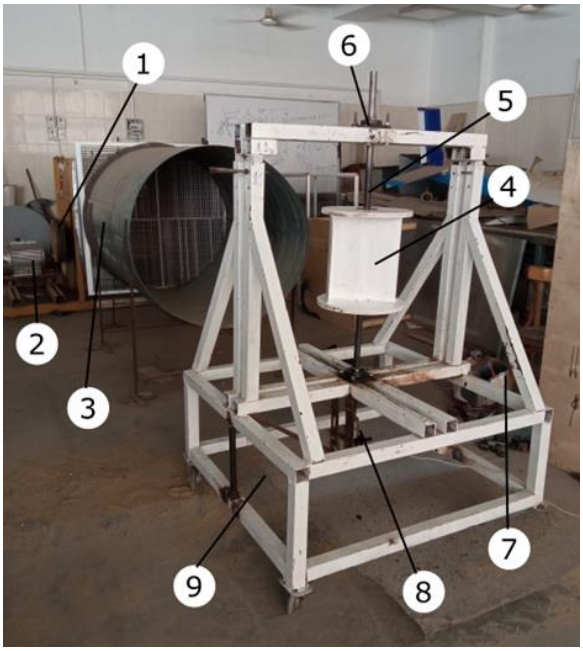

Figure.7- Experimental setup used to measure the performance of wind turbine

Figure 8- Three-dimensional plot and a photograph of the fabricated Savonius rotor, Model M4

5. Results and Discussion

5.1 Numerical results

The effect of rotor blade profile on the turbine performance is shown in Figure 9. The performance of rotor model M1 shows a higher power coefficient. The tip speed ratio at optimum condition is shrunk out, as compared to Model 2.

The numerical simulations are then performed on M3 and compared with M1, Figure 10 with the same profile but with different thicknesses. The results show better performance for thinner-blade rotor M3.

The thinner blade has less deformation in the profile equation obtained at its centerline. Furthermore, the tip loss is expected to be less. These may be the reasons to obtain higher performance for thinner blade. The simulations are performed also on M3, M4, M5, and M6 rotor models of different blade profiles with the same blade thickness of 2 mm Figure 11. The comparisons reveal that the model M4 has the highest power coefficient as the blade is hooked outwards. The peak power coefficient is 0.164 at λ = 0.55. However, the rotor model, M6, has the closer performance to M5 with an extended operating tip speed ratio for maximum performance.

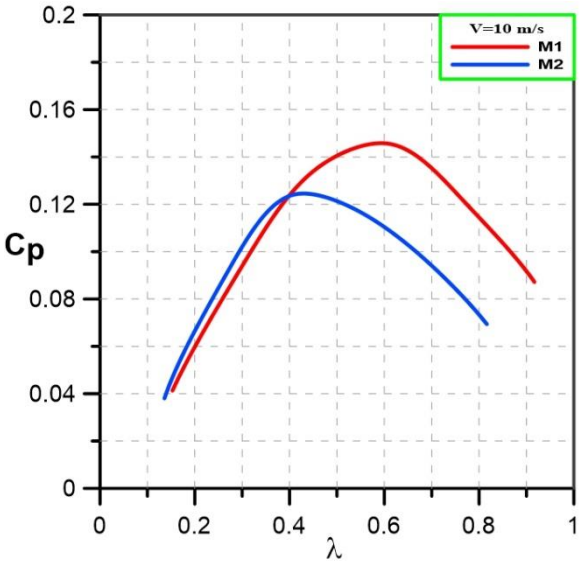

Figure 9- Comparison of wind turbine performance in terms of C_p for models M1 and M2

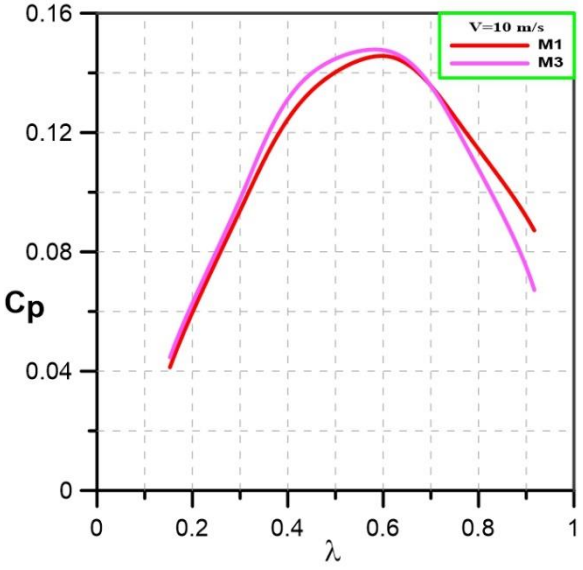

Figure 10- Comparison of wind turbine performance in terms of C_p for models M1 and M3

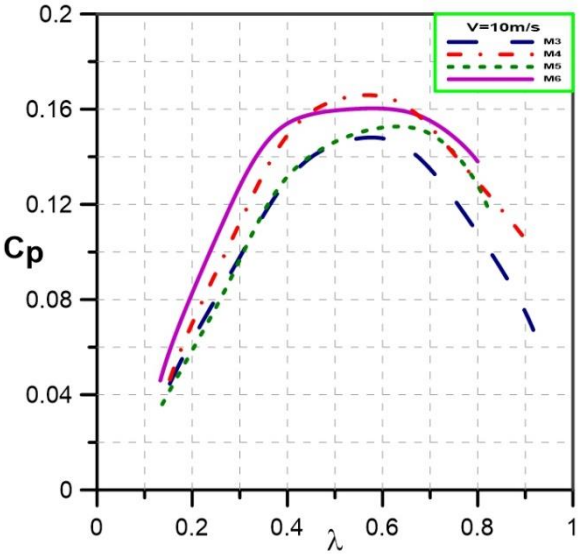

Figure 11- Comparison of wind turbine performance in terms of C_p for models M3, M4, M5 and M6

Figure 12 shows the variation of the torque coefficient with rotor rotation over a half revolution for the six tested rotor models, at tip speed ratios of λ = 0.4 and λ = 0.6. It is observed that at (λ = 0.4) M3 has the highest value of the torque coefficient as compared to M1, and M2, despite, M2 having the lowest average value of the torque coefficient. On the second hand, it is found that M6 has the highest value of the torque coefficient as compared to M4, M5, while M5 has the lowest value of the torque coefficient in the first half of half-cycle, M4 has the lowest value of the torque coefficient at the second half of half cycle. at (λ = 0.6) it is found that M3 has the highest value of the torque coefficient in the first half of half-cycle, M1 has the highest value of the torque coefficient in the second half of half-cycle while M2 has the lowest average value of the torque coefficient over half cycle. On the second hand it is found that M6 has the highest value of the torque coefficient as compared to M5, M4, while M6 has the lowest value of the torque coefficient in the first half of half-cycle at $\theta = 75^{\circ}$, M4 has the lowest value of the torque coefficient at the second half of half cycle.

An important parameter to measure the starting ability of the rotor is the static torque coefficient (CT_s). Figure 13 shows the static torque coefficient

of the six rotor models at different rotor orientations (θ). The rotor model M2 shows negative static torque coefficient in the range of $\theta = 105^{\circ}$ to $\theta = 180^{\circ}$. Furthermore, model M3 shows CT_s close to zero with minimum at rotor angle of 150°. Moreover, M3 has a significant rise in the static torque coefficient at wide range of rotor orientations up to $\theta = 90^{\circ}$. The maximum value of static torque coefficient for M1 and M2 occurs at rotor angle of $\theta = 45^{\circ}$, while M1 has maximum value at $\theta = 0^{\circ}$ and $\theta = 180^{\circ}$. The results reveal that the rotor models M4, M5 and M6 have positions CT_s for all orientations, which indicate high starting ability. The minimum values of CT_s obtained for M4, M5 and M6 are higher than the corresponding minimum value of rotor Models M4. It can be concluded that the rotors models M4, M5 and M6 has good starting ability with starting superiority to models M4 and M6.

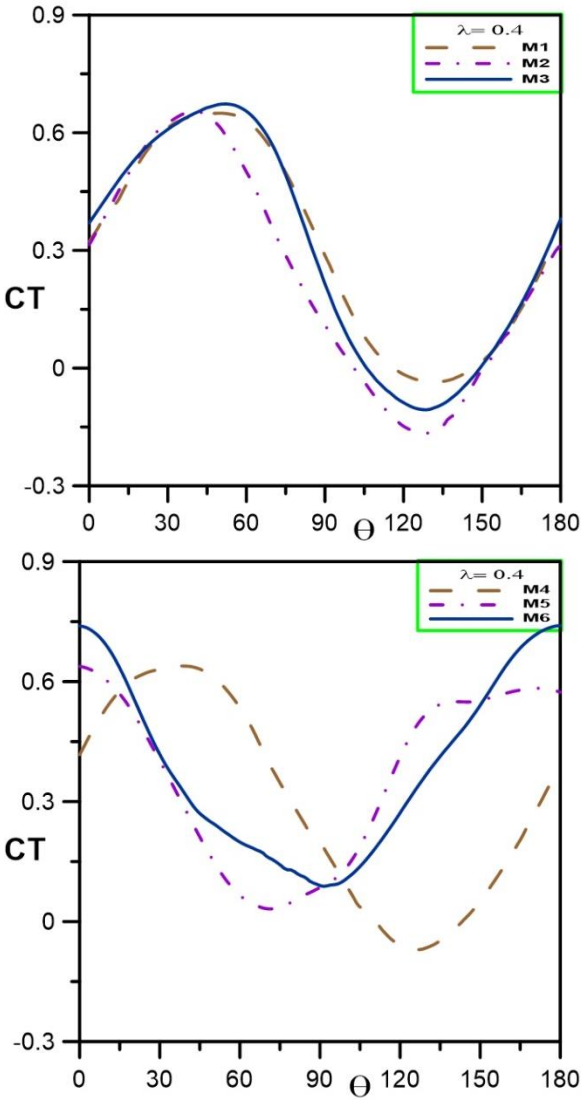

(a) Tip speed ratio $\lambda = 0.4$

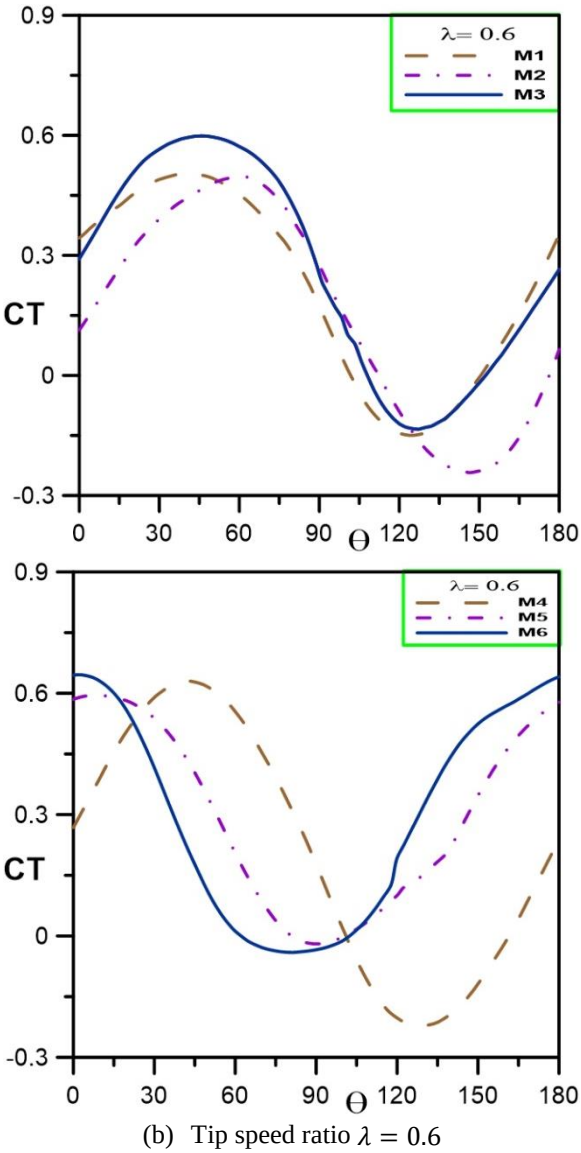

(b) Tip speed ratio $\lambda = 0.6$

Figure 12- Variation of instantaneous torque coefficient with rotor rotation

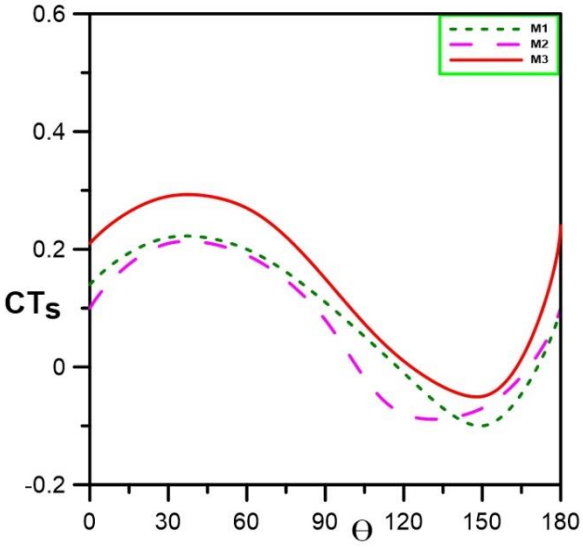

(a). Models M1, M2, and M3

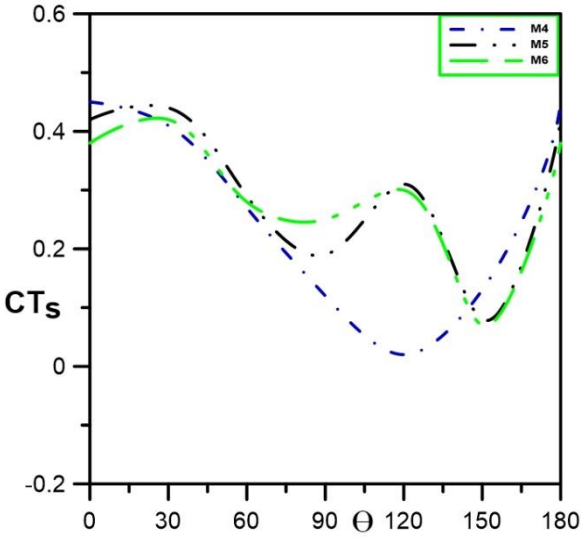

(b). Models M4, M5 and M6

Figure 13- Static torque coefficient obtained at different rotor orientations for the six rotor models

The flow characteristics of the tested rotor models in terms of pressure and streamline contours are explored in Figs .14 and 15, respectively. The results are presented through a sectional top view at the middle height of the rotors, compared to the other tested rotors, Model M4 has relatively lower pressure on the front surface of the returning blade at a rotor angle of 0°, with almost similar pressure on the front of the advancing blade of all rotors. This reduces the negative drag created on the M4 rotor. Further, the negative pressure arising on the backside of the advancing blade at rotor angle θ = 90° covers extended region, see Figure 15. There is also a relatively higher pressure observed on the advancing blade of Model M4 as compared to other rotor models.

Consequently, the average positive drag created on the M4 is higher, as reflected on the rotor performance presented previously in Figure 11. The wind flow hitting the advancing blade at the same level of the arm, M1, M3, M4, the flow outwards as shown in Figure14–i. This directs consequently the reduce of the force created on the returning blade. At rotor angle θ = 90° presented in Figure 14-ii, the vortices created behind the rotor increases the turbulence fluctuations over the rotor and reduces its performance.

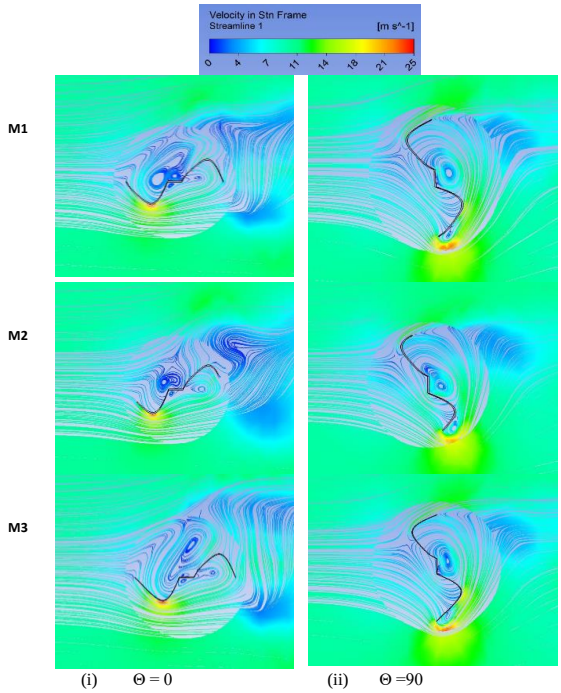

Figure 14- Velocity streamlines of different models at two orientations of Savonius rotor, θ = 0° and θ =90°

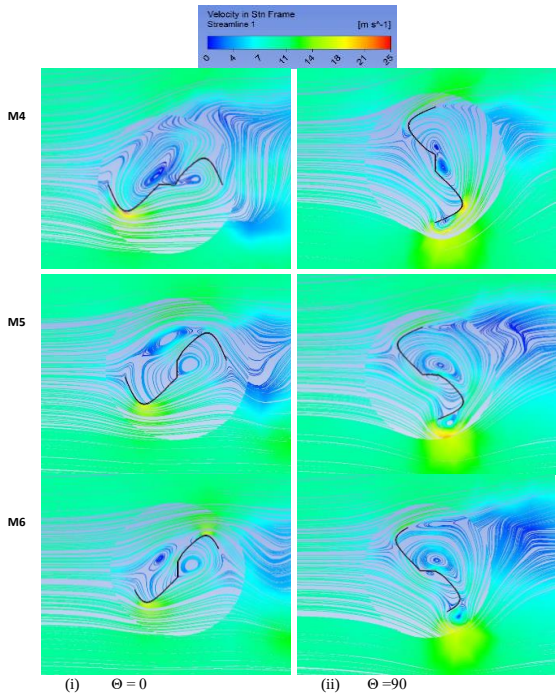

Figure 14- (continued):
Velocity streamlines of different models at two orientations of Savonius rotor, θ = 0° and θ =90°

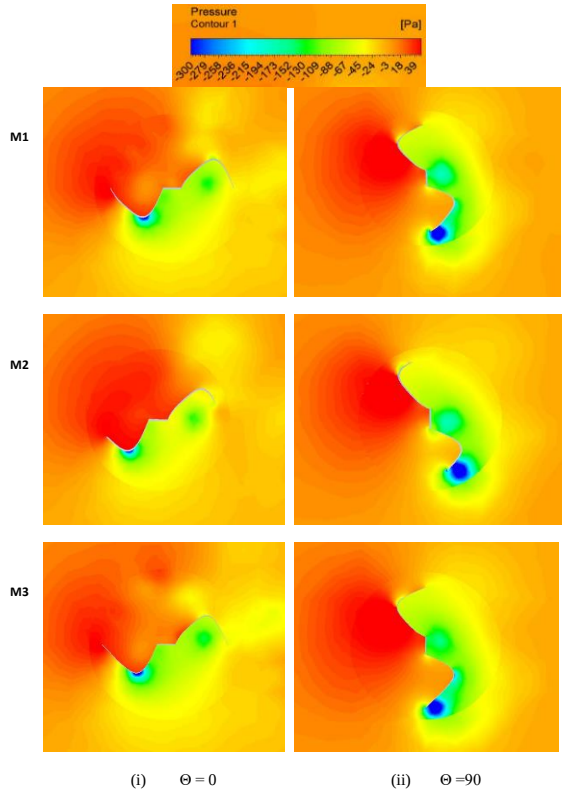

Figure 15- Pressure contours of different models at two orientations of Savonius rotor, θ = 0° and θ =90°

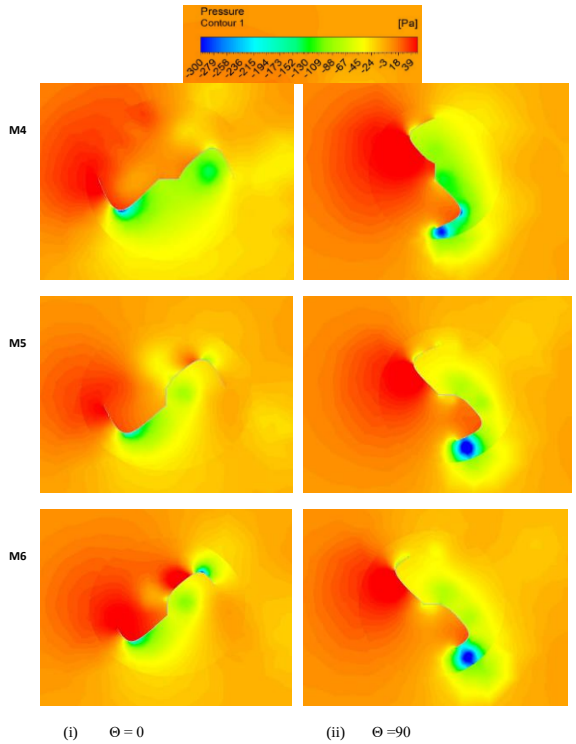

Figure 15- (continued):
Pressure contours of different models at two orientations of Savonius rotor, θ = 0° and θ =90°

5.2. Comparison with the present experimental results

From the numerical results, Model M4 has a better performance compared with the other models. Therefore, the wind turbine rotor model 4, has been fabricated and tested under different operational conditions. The rotor performance is presented in Figures 16, to 18 in terms of power coefficient versus tip speed ratio. The rotor is observed to have slightly better performance at a lower wind speed of 8 m/s. Furthermore, the peak performance is shifted towards a lower tip speed ratio, for higher wind speed with shrunk operating range. It is found also that; the numerical simulations predict well the average rotor performance.

6. Conclusions

This research aims to test the performance of modified Savonius blades with different arm-bucket orientations. The numerical simulations are validated with available experimental data from literature and

present a fabricated rotor model. Six rotor models are introduced and the effects of blade thickness, bucket profile, and orientation are explored. The rotor model M4 of parallel arm-buckets achieves the highest power coefficient. The increase in blade thickness is found to have a negative effect on the rotor behavior with a reduced power coefficient. The experimental measurements on the M4 model show better performance of the rotor at low wind speed.

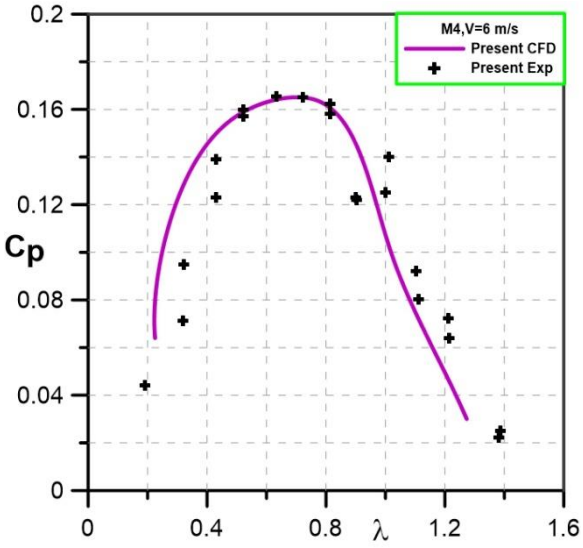

Figure 16- Comparison of power coefficient between the present experiments and numerical simulation results, V = 6 m/s

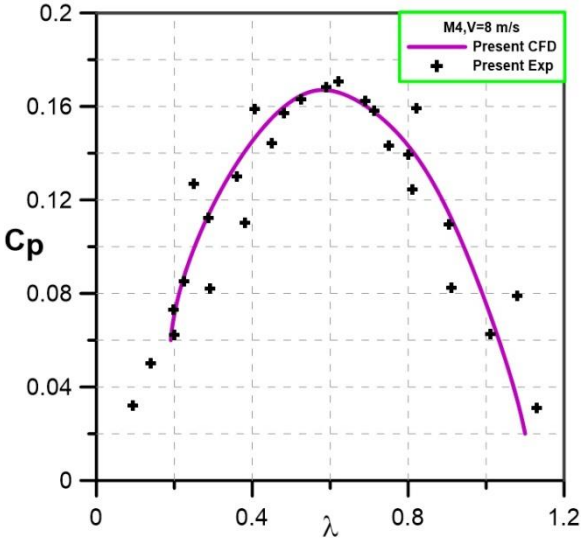

Figure 17- Comparison of power coefficient between the present experiments and numerical simulation results, V =8 m/s

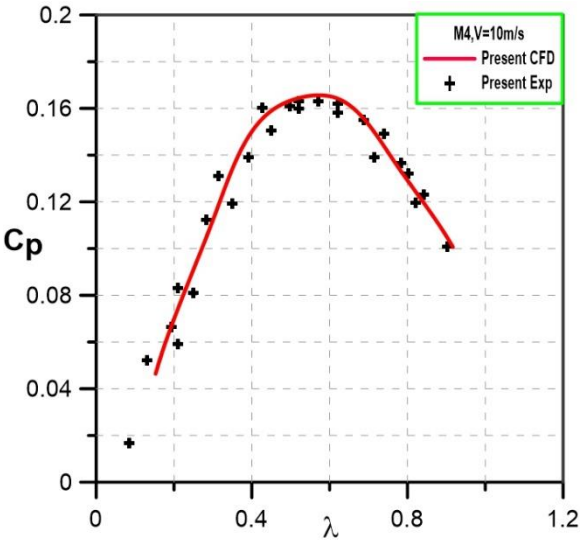

Figure 18- Comparison of power coefficient between the present experiments and numerical simulation results, V =10 m/s

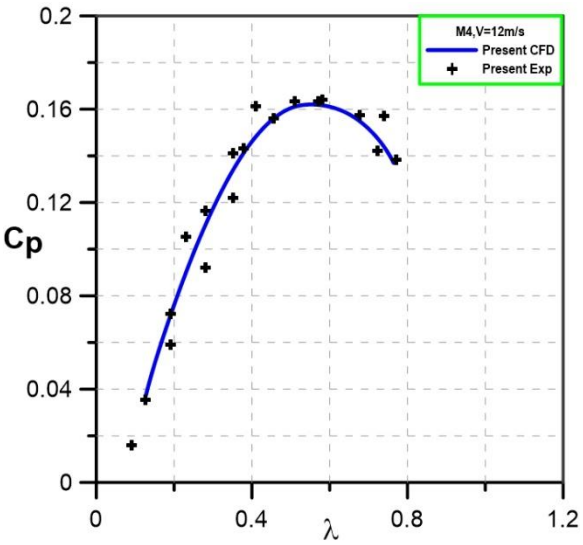

Figure 19- Comparison of power coefficient between the present experiments and numerical simulation results, V =12 m/s

7. Nomenclature:

A	Area of wind turbine rotor (m^2)
AR	Aspect ratio
$_pC$	(٢AVρ٠.٥T/(Ω= Power coefficient
$_TC$	(H٢V٢Dρ)/T٤=coefficient Torque
D	(otor diameter (mR
$_oD$	(End plate diameter (m
H	(otor height (mR
T	(Rotor torque (N.m
V	Free stream wind speed (m/s)

ρ	Air density (kg/m^3)
Ω	(rad/s) Angular velocity
λ	Tip speed ratio of rotor = Ω D/2V
θ	Rotation angle of the rotor (°)

8. References

[1] N.H. Mahmoud, A.A. El-Haroun, E. Wahba and M.H. Nasef, "An experimental study on improvement of Savonius rotor performance", Alexandria Engineering Journal, vol. 51,2012, pp. 19–25.

[2] J.V. Akwa, H. A. Vielmo and A. P. Petry, "A review on the performance of Savonius wind turbines", Renewable and Sustainable Energy Reviews, vol. 16, 2012, pp. 3054–3064.

[3] W.A. El-Askary, A. S. Saad, A.M. Abdelsalam and I.M. Sakr, "Investigating the performance of a twisted modified Savonius rotor", Journal of Wind Engineering & Industrial Aerodynamics, vol. 182, 2018, pp. 344–355.

[4] A. Damak, Z. Driss, M.S. Abid, "Experimental investigation of helical Savonius rotor with a twist of 180", Renewable Energy, vol. 52, 2013, pp. 136–142.

[5] A. Al-Faruk and A. Sharifian, "Flow field and performance study of vertical axis Savonius type SST wind turbine", Energy Procedia, vol. 139, 2017, pp. 235–242.

[6] J. H. Lee, Y. T. Lee, and H. C. Lim, "Effect of twist angle on the performance of Savonius wind turbine", Renewable. Energy, vol. 89, 2016, pp. 231–244.

[7] K. Kacprzak, G. Liskiewicz and K. Sobczak, "Numerical investigation of conventional and modified Savonius wind turbines", Renewable Energy, vol. 60, 2013, pp. 578–585.

[8] S. Roy and U. K. Saha, "Wind tunnel experiments of a newly developed two-bladed Savonius-style wind turbine", Applied Energy, vol. 137, 2015, pp. 117–125.

[9] A. Damak, Z. Driss and M.S. Abid, "Optimization of the helical Savonius rotor through wind tunnel experiments", Journal of Wind Engineering & Industrial Aerodynamics, vol. 174 , 2018, pp. 80–93.

[10] N. Alom and U.K. Saha, "Evolution and Progress in the Development of Savonius Wind Turbine Rotor Blade Profiles and Shapes", Journal of Solar Energy Engineering, 141(3), 2019, pp: 030801.

[11] M.H. Pranta, M.S. Rabbi, M.M. Roshid, "A computational study on the aerodynamic performance of modified Savonius wind turbine", Results in Engineering, 10, 2021, pp: 100237.

[12] I. Marinić-Kragić , D. Vučina and Z. Milas, "Global optimization of Savonius-type vertical axis wind turbine with multiple circular-arc blades using validated 3D CFD model", Energy, 241, 2022, pp:122841.

[13] S. Torres, A. Marulanda, M.F. Montoya, C. Hernandez, "Geometric design optimization of a Savonius wind turbine", Energy Conversion and Management, 262, 2022, pp: 115679.

[14] N. Cuevas-Carvajal, J.S. Cortes-Ramirez, J.A. Norato, C. Hernandez, M.F. Montoya-Vallejo, "Effect of geometrical parameters on the performance of conventional Savonius VAWT: A review", Renewable and Sustainable Energy Reviews, vol. 161, 2022, pp: 112314.

[15] H. E. Gad, A. A. Abd El-Hamid, W.A. El-Askary, and M. H. Nasef, "A New Design of Savonius Wind Turbine: Numerical Study", CFD Letters, vol. 6, no. 4, 2014, pp. 144–158.

[16] E.P. Wolfe and S.S. Ochs, "CFD calculations of S809 aerodynamic characteristics", AIAA aerospace sciences meeting; 1997.

[17] K. Hamada, T. Smith, N. Durrani, N. Qin, and R. Howell, "Unsteady flow simulation and dynamic stall around vertical axis wind turbine blades", AIAA aerodynamics conference Reno, 2008.

[18] R. Howell, N. Qin, J. Edwards and N. Durran, "Wind tunnel and numerical study of a small vertical axis wind turbine", Renewable Energy, vol. 35, 2010, pp. 412–422.

[19] A.M. Abdelsalam, and V. Ramalingam, "Wake prediction of horizontal-axis wind turbine using full-rotor modeling", J. Wind Eng. Ind. Aerodyn, 12, 2014, pp. 7-19.

[20] A.M. Abdelsalam, K. Boopathi, S. Gomathinayagam, SS. Kumar, and V. Ramalingam, "Experimental and numerical studies on the wake behavior of a horizontal axis wind turbine", J. Wind Eng. Ind. Aerodyn, 128, 2014, pp. 54–65.

[21] A.M. AbdelSalam, W.A. El-Askary, M.A. Kotb, I.M. Sakr, "Experimental study on small scale horizontal axis wind turbine of analytically-optimized blade with linearized chord twist angle profile", Energy, 216, 2021: 119304.